



Experimental Investigation of a Seamlessly Converged Fiber-Wireless Access Network Employing Free-Running Laser- and Envelope Detection-based mmWave Generation and Detection

Vallejo Castro, Luis; Gonem, Omaro; Jin, Wei; Faruk, Md Saifuddin; Giddings, Roger; Yi, Xingwen; Tang, Jianming

Optics Express

DOI:
[10.1364/OE.532694](https://doi.org/10.1364/OE.532694)

Published: 07/01/2025

Publisher's PDF, also known as Version of record

[Cyswllt i'r cyhoeddiad / Link to publication](#)

Dyfyniad o'r fersiwn a gyhoeddwyd / Citation for published version (APA):
Vallejo Castro, L., Gonem, O., Jin, W., Faruk, M. S., Giddings, R., Yi, X., & Tang, J. (2025). Experimental Investigation of a Seamlessly Converged Fiber-Wireless Access Network Employing Free-Running Laser- and Envelope Detection-based mmWave Generation and Detection. *Optics Express*, 33(1), 604-618. <https://doi.org/10.1364/OE.532694>

Hawliau Cyffredinol / General rights

Copyright and moral rights for the publications made accessible in the public portal are retained by the authors and/or other copyright owners and it is a condition of accessing publications that users recognise and abide by the legal requirements associated with these rights.

- Users may download and print one copy of any publication from the public portal for the purpose of private study or research.
- You may not further distribute the material or use it for any profit-making activity or commercial gain
- You may freely distribute the URL identifying the publication in the public portal ?

Take down policy

If you believe that this document breaches copyright please contact us providing details, and we will remove access to the work immediately and investigate your claim.



Experimental investigation of a seamlessly converged fiber-wireless access network employing free-running laser- and envelope detection-based mmWave generation and detection

LUIS VALLEJO,^{*}  OMARO FAWZI ABDELHAMID GONEM,  WEI JIN,  MD SAIFUDDIN FARUK,  ROGER PHILIP GIDDINGS,  XINGWEN YI,  AND JIANMING TANG 

Digital Signal Processing Centre of Excellence, School of Computer Science and Engineering, Bangor University, Bangor LL57 1UT, United Kingdom

^{*}*l.vallejocastro@bangor.ac.uk*

Abstract: Employing free-running laser/envelope detection-based millimeter wave (mmWave) signal generation/detection at remote radio heads (RRHs)/user equipment (UE) offers a cost-effective solution for seamlessly integrating existing intensity modulation-direct detection (IM-DD)-dominated optical access networks and wireless networks. Such fiber-wireless convergence enables a continuous flow of signals with varying characteristics between the baseband unit (BBU) and UE across fiber and wireless network segments without the need for optical-electrical-optical (O-E-O) conversions and digital signal processing (DSP) at intermediate nodes. In this paper, we extensively investigate the performance of such a fiber-wireless converged access network employing free-running laser/envelope detection-based mmWave generation/detection in an IM-DD-based 1.67 Gbit/s transmission system with 25 km standard single-mode fiber (SSMF) and 5 m @38 GHz mmWave wireless links. Experimental results demonstrate that both mmWave frequency tunability and adaptive mmWave network coverage are achievable by just dynamically and adaptively configuring the output wavelength and power of the RRH-embedded free-running laser. Additionally, envelope detection allows RRHs to use low-cost MHz-linewidth-level free-running lasers while maintaining excellent performance stability.

Published by Optica Publishing Group under the terms of the [Creative Commons Attribution 4.0 License](https://creativecommons.org/licenses/by/4.0/). Further distribution of this work must maintain attribution to the author(s) and the published article's title, journal citation, and DOI.

1. Introduction

The continuous proliferation of HD/UHD video applications, interactive network services, mobile cloud services, and machine-to-machine (M2M) communications has led to an explosive increase in global mobile traffic, which is expected to reach 465 exabytes (EB) per month by 2030 [1]. To meet these expectations, beyond-fifth-generation (B5G) mobile networks are therefore required to offer unprecedented peak data rates of ≥ 1 Tbps with ultra-low latencies of 10–100 μ s, and massive connection densities of 10 million devices/km² [2]. This imposes unprecedented challenges on B5G mobile access networks in terms of not only delivering high throughput, low latency, and extensive coverage, but also offering high network flexibility, adaptability, scalability, and upgradability in a cost-effective manner [3].

The seamless convergence of fiber and wireless network segments is highly advantageous to achieve the above challenging goals of B5G mobile networks [4,5], as such convergence enables signals with varying characteristics, such as bandwidth and modulation formats, to

seamlessly and continuously flow across the entire mobile access network, i.e., between the baseband unit (BBU) and user equipment (UE), regardless of carrier domains (optical and/or electrical domains), without requiring optical-electrical-optical (O-E-O) conversions or extensive digital signal processing (DSP) at intermediate nodes. Considering the fact that millimeter wave (mmWave) wireless communications, introduced in the 5G new radio (NR) standard [6], will remain crucial in the B5G era to support services and applications requiring ultra-high bandwidth/capacity and ultra-low latency [7,8], thus, simple, cost-effective, and tunable mmWave signal generation and detection approaches are vital to effectively implement such highly desirable seamless fiber-wireless access network convergence [4,5,9].

Various mmWave generation/detection techniques have been proposed, whose technical comparisons are presented in Table 1. Generally speaking, employing electronic components for mmWave signal up-conversion and down-conversion is not a cost-effective approach as the electronic components are restricted by their inherent limited bandwidth and cannot cost-effectively offer required mmWave frequency tunability within a wide frequency range, which is desirable for considerably enhancing mobile networks' flexibility/adaptability [5,10]. In comparison, photonics-aided mmWave signal generation approaches are attractive due to the broadband bandwidth of commercially available optical components [11,12,13]. For these techniques, mmWave signal generation mainly relies on the optical beating of two wavelengths in a photodetector (PD) where the wavelength spacing determines the produced mmWave carrier frequency. Several photonics-aided mmWave signal generation techniques have been demonstrated based on phase locking [14,15,16] or using multimode optical sources [17,18]. In addition, external optical modulators can also be used to generate the required two beating optical signals, for example, intensity and phase modulation-produced harmonic components [19,20]. Furthermore, the optical non-linear effects such as four-wave mixing (FWM) and stimulated Brillouin scattering (SBS) [21,22] can also be incorporated into the above external modulator-based techniques for achieving higher frequency mmWave signals. However, all the above-mentioned mmWave generation techniques are relatively complex and uneconomical for applications in cost-sensitive access network scenarios.

For producing the required two beating optical signals, photonics-aided mmWave signal generation approaches using two independent lasers, here known as the free-running laser technique, are promising due to their simplicity and high cost-effectiveness [11,23,24,25]. For practical implementations, one free-running laser is used at the BBU for transmitting user data to the remote radio head (RRH), whereas the other free-running laser can be hosted at the RRH to produce the desirable mmWave signal via the optical beating of the RRH-laser output and the BBU-transmitted optical signal received at the RRH [26,27]. This infrastructure not only enables the reuse of the RRH-laser sources for upstream transmissions, but also results in a reduction in the overall optical powers launched into the fiber, which, as a direct result, reduces the associated fiber nonlinearity effects, eliminates fiber transmission-induced optical power loss, and further enhances the overall network power utilization efficiency. However, for the free-running laser-based mmWave signal generation approach, the generated mmWave signal suffers high phase noise and frequency drifting (also known as frequency offset) effects due to the beating of the two independent optical signals. To address this issue, a cost-effective electrical passive envelope detector (ED) can be employed at the UE receiver for down-converting the mmWave signal to the baseband spectral region. Such mmWave down-conversion is insensitive to the mmWave carrier phase noise and frequency drifting effects, thus the deployment of the ED at the UE enables the UE receiver to use conventional DSP techniques for signal demodulation without phase noise and frequency drifting estimation and compensation [5,24,25].

The technical feasibility of the free-running laser/envelope detection-based mmWave signal generation/detection has been respectively demonstrated in optical single-sideband modulation (I/Q modulation) links [28,29,30,31] and double-sideband modulation (intensity modulation,

Table 1. Comparisons between different mmWave signal generation/detection techniques.^a

Ref.	Technique	Technical comparison
[10] [33]	Electrical up-conversion	<p>Advantage: low bandwidth PDs are required for O-E conversion.</p> <p>Complexity: high-bandwidth electrical components (LOs, multipliers, mixers, etc.) are required.</p> <p>Frequency tunability: constrained by electrical LO tunability.</p> <p>Adaptive wireless coverage: N/D.</p> <p>UE Rx: signal down-conversion using either i) an electrical LO [10,33]; or ii) an electrical envelope detection [10].</p> <p>UE DSP: with [10] and without [33] PN and FO estimation and compensation.</p>
[14] [34]	Injection locking	<p>Advantage: generation of mmWave signals with reduced PN and FO.</p> <p>Complexity: high-quality optical sources and high-bandwidth PDs are required with limited locking range and injection power control.</p> <p>Frequency tunability: by adjusting master-slave lasers' wavelengths.</p> <p>Adaptive wireless coverage: N/D.</p> <p>UE Rx: electrical envelope detection for signal down-conversion.</p> <p>UE DSP: without PN and FO estimation and compensation.</p>
[17] [35] [36]	Dual-wavelength lasers	<p>Advantage: generation of mmWave signals with reduced PN and FO.</p> <p>Complexity: special lasers such as common cavity dual-mode and fiber-ring lasers, and high-bandwidth PDs are required.</p> <p>Frequency tunability: constrained by the wavelength spacing between optical modes.</p> <p>Adaptive wireless coverage: N/D.</p> <p>UE Rx: analog signal down-conversion using an electrical LO.</p> <p>UE DSP: without PN and FO estimation and compensation.</p>
[18] [37]	Integrated on-chip laser sources	<p>Advantage: generation of mmWave signals with reduced PN and FO.</p> <p>Complexity: special laser chip (two lasers integrated on the same chip) and high-bandwidth PDs are required.</p> <p>Frequency tunability: by adjusting the current injection or thermal tuning.</p> <p>Adaptive wireless coverage: N/D.</p> <p>UE Rx: signal down-conversion using either i) an electrical LO-free PNC receiver [18]; or ii) an electrical envelope detection [18].</p> <p>UE DSP: without PN and FO estimation and compensation [18].</p>
[19] [20] [38] [39] [40] [41]	External modulation	<p>Advantage: generation of mmWave signals with reduced PN and FO.</p> <p>Complexity: requires high-bandwidth external modulators, RF sources and PDs.</p> <p>Frequency tunability: limited by launched RF sources.</p> <p>Adaptive wireless coverage: N/D.</p> <p>UE Rx: analog signal down-conversion using an electrical LO.</p> <p>UE DSP: without PN and FO estimation and compensation.</p>
[5] [25] [42]	Free-running lasers (two lasers at CO-BBU)	<p>Advantage: laser-free RRH.</p> <p>Complexity: requires high-bandwidth PDs and high BBU optical launch power, suffers from high fiber power loss.</p> <p>Frequency tunability: by adjusting CO-BBU-lasers' wavelengths.</p> <p>Adaptive wireless coverage: N/D.</p> <p>UE Rx: signal down-conversion using either i) an electrical LO-free PNC receiver [25]; or ii) an electrical envelope detection [5,25,42].</p> <p>UE DSP: without PN and FO estimation and compensation.</p>
[23] [28] [43] [44] [45] [46] [47] This work	Free-running lasers (one laser at RRH)	<p>Advantage: low fiber power loss, low BBU optical launch power [This work], excellent mmWave frequency tunability [This work], adaptive wireless coverage [This work] and significant transmission performance improvements induced by high RRH-laser powers [This work].</p> <p>Complexity: requires high-bandwidth PDs and RRH-laser control.</p> <p>Frequency tunability: by adjusting RRH-laser wavelengths [This work].</p> <p>Adaptive wireless coverage: by just adjusting RRH-laser output powers [This work].</p> <p>UE Rx: signal down-conversion using either i) an electrical LO [23,28,44,45,47]; ii) digital down-conversion [43] or envelope detection [28] with high-speed ADCs ; iii) electrical envelope detector [46] with low-speed ADCs [This work].</p> <p>UE DSP: demodulation with [23,28,43,44,45,47] and without [46] and [This work] PN and FO estimation and compensation.</p>

^aNote: PD: photodetector, RRH: remote radio head, CO-BBU: central office-baseband unit, Rx: receiver, PN: phase noise, FO: frequency offset, O-E: opto-electronic conversion, PNC: phase noise cancellation, N/D: not discussed, LO: local oscillator, ADC: analog-to-digital converter.

IM) links [5,24,32]. Among these approaches, mmWave signal generation/detection based on IM links is highly advantageous because existing optical access networks rely extensively on intensity modulation-direct detection (IM-DD) links. This makes the integration of IM-based free-running laser/envelope detection-enabled mmWave signal generation/detection techniques not only cost-efficient but also seamlessly upgradable with the current optical access network architectures. However, for practically implementing the free-running laser and envelope detection-based mmWave generation and detection technique, comprehensive investigations are still required to identify optimum free-running laser conditions, and more importantly, to evaluate the associated network performance trade-offs between robustness, stability, mmWave tuning ranges and wireless coverage.

To deliver the abovementioned objectives, in this paper, we experimentally investigate the performance of a 1.67 Gbit/s seamlessly converged fiber-wireless access network employing free-running laser/envelope detection-based mmWave generation/detection in an IM-DD-based transmission system with 25 km standard single-mode fiber (SSMF) and 5 m @38 GHz mmWave wireless links. The experimental results show that, by incorporating a free-running laser with dynamic control of output wavelength and power at the RRH, several additional salient features are achievable, including i) excellent mmWave frequency tunability by simply adjusting the RRH-laser wavelength, as verified in Section 4.2; ii) the ability of enhancing the transmission performance and also allowing the BBU to launch relatively low optical powers for mitigating the fiber nonlinearity effects, as verified in Section 4.3; iii) adaptable mmWave wireless coverage and great potential of extending the wireless coverage beyond 45 m by simply changing the RRH-laser optical power, as verified in Section 4.4; and iv) the reuse of the RRH-lasers for upstream transmissions for reducing the overall network expenditures. Additionally, the experimental results also show the excellent performance stability and robustness of the proposed fiber-wireless converged access networks against the RRH-laser linewidth and frequency drifting, this allows the RRHs to use low-cost MHz-linewidth-level free-running lasers to reduce the overall network capital expenditure, as demonstrated and verified in Section 4.5.

2. Seamlessly converged fiber-wireless access networks

The seamlessly converged fiber-wireless access network architecture employing free-running laser/envelope detection-based signal generation/detection is illustrated in Fig. 1, where at the RRH, no O-E-O conversions and no DSP are implemented, thus enabling signals of various characteristics to continuously flow between the BBU and UE with minimal latency.

In this network architecture, at the BBU, an optical signal employing an arbitrary modulation format is generated via IM and transmitted over the SSMF to RRHs. The BBU-generated optical signal can be expressed as:

$$S_{BBU}(t) = \sqrt{P_{BBU}} \sqrt{1 + m \cdot s(t)} e^{j(\omega_{BBU}t + \varphi_{BBU}(t))}, \quad (1)$$

where P_{BBU} is the optical signal power, ω_{BBU} is the optical signal angular frequency, and $\varphi_{BBU}(t)$ denotes the phase noise of the central office (CO)-located BBU-laser. m is the intensity modulation index, and $s(t)$ is the real-valued transmitted data signal supporting an arbitrary modulation format.

After fiber transmissions, at the RRH, the optical signal is first passively coupled with an optical carrier signal locally generated by a standalone free-running laser diode (LD)-2. Assuming a fiber transmission system suffering a linear loss only, the total combined signal can be expressed as:

$$S_T(t) = \sqrt{\alpha} S_{BBU}(t) + S_{RRH}(t), \quad (2)$$

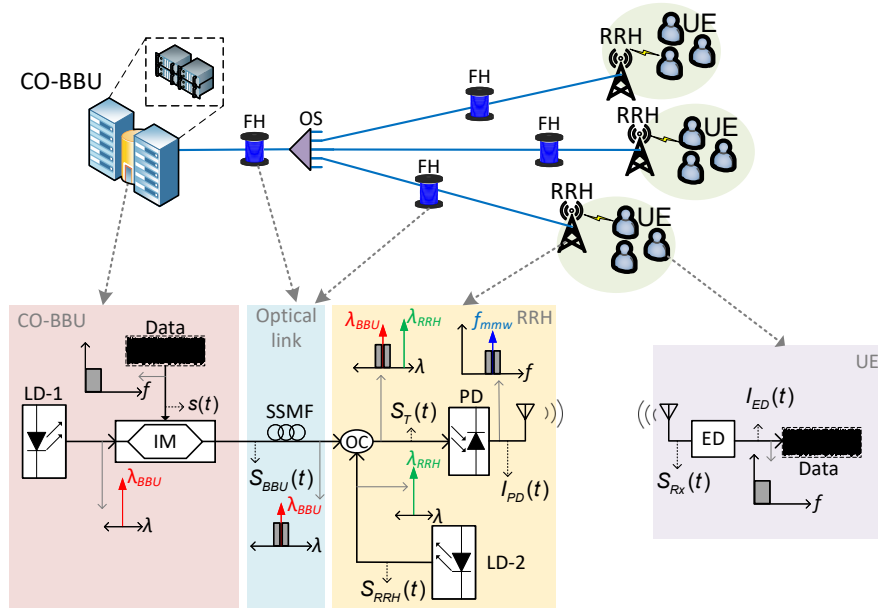


Fig. 1. Seamlessly converged fiber-wireless access network architecture based on intensity modulation links and free-running laser/envelope detection-based mmWave signal generation/detection. CO-BBU: central office-baseband unit, FH: fronthaul, OS: optical splitter, RRH: remote radio head, UE: user equipment, LD: laser diode, IM: intensity modulator, SSMF: standard single-mode fiber, OC: optical coupler, PD: photodetector, ED: envelope detector.

where α is the scaling factor representing the fiber transmission link-induced power loss. $S_{RRH}(t)$ is the RRH locally generated optical signal which can be written as:

$$S_{RRH}(t) = \sqrt{P_{RRH}} e^{j(\omega_{RRH}t + \varphi_{RRH}(t))}, \quad (3)$$

where P_{RRH} is the optical signal power, ω_{RRH} is the optical signal angular frequency, and $\varphi_{RRH}(t)$ denotes the phase noise of the RRH-laser. The RRH-laser is adjusted so that the frequency difference between the BBU-laser and the RRH-laser equals the targeted mmWave angular frequency $\omega_{mmW} = |\omega_{BBU} - \omega_{RRH}|$.

The two combined optical signals are then directed to the RRH-PD to generate the desired mmWave signal via optical beating. Assuming an ideal PD for simplicity, the process can be expressed as:

$$\begin{aligned} I_{PD}(t) &= |S_T(t)|^2 \\ &= \alpha P_{BBU} + P_{RRH} + m\alpha P_{BBU} s(t) + 2\sqrt{\alpha P_{BBU} P_{RRH}} \sqrt{1 + m \cdot s(t)} \cos(\omega_{mmW}t + \Delta\varphi(t)), \end{aligned} \quad (4)$$

where $\Delta\varphi(t) = \varphi_{BBU}(t) - \varphi_{RRH}(t)$, which denotes the total phase noise.

In Eq. (4), the first two terms are the direct current (DC) terms whereas the third term is the signal at the baseband region. The fourth term is the desired mmWave signal to be transmitted to the UEs. When the first three terms are not spectrally overlapped with the desired mmWave signal, they can be removed by electronic band-pass or high-pass filtering. Assuming an ideal band/high-pass filtering operation, after wireless transmissions, the UE-received mmWave signal

can be expressed as:

$$S_{Rx}(t) = 2\sqrt{\gamma}\sqrt{\alpha P_{BBU}P_{RRH}}\sqrt{1+m \cdot s(t)} \cos(\omega_{mm}Wt + \Delta\varphi(t)), \quad (5)$$

where γ is a scaling factor representing the signal power loss due to the wireless link. Equation (5) indicates that the UE-received mmWave signal suffers high phase noise. The UE receiver uses a square-law ED to directly down-convert the received mmWave signal to the baseband spectral region, which can be expressed as:

$$\begin{aligned} I_{ED}(t) &= |S_{Rx}(t)|^2 \\ &= 2\gamma\alpha P_{BBU}P_{RRH} + 2m\gamma\alpha P_{BBU}P_{RRH}s(t) \\ &\quad + 2\gamma\alpha P_{BBU}P_{RRH}(1+m \cdot s(t)) \cos(2\omega_{mm}Wt + 2\Delta\varphi(t)). \end{aligned} \quad (6)$$

The first term in Eq. (6) is the DC term. The second term is the desirable signal which is already down-converted to the baseband spectral region, whereas the third term is the unwanted high-frequency component. When the third term does not overlap with the desired signal term, the third term can be easily removed by low-pass filtering. From Eq. (6), the ED can perform the mmWave signal down-conversion operation, which is insensitive to the unwanted phase noise and frequency drifting arising from the optical beating [25]. After the ED, the UE receiver can employ an analog-to-digital converter (ADC) operating just at the bandwidth of the transmitted signal and use conventional DSP techniques for signal demodulation without the need to use complicated DSP algorithms to mitigate the frequency drifting and phase noise effects.

It is also interesting to mention that, as shown in Eq. (5) and Eq. (6), the power of the produced mmWave signal and the power of the UE-received desired signal are strongly related to both the RRH-received optical signal power and the RRH-laser output power. Dynamic RRH-laser power adjustments are thus applicable for adaptively adjusting the produced mmWave signal power for enhancing the transmission performance and also for achieving a flexible mmWave coverage. In addition, this also relaxes the stringent requirements on high-gain optical/electrical amplifiers. This also potentially allows the BBU to launch optical signals of relatively low powers into the fiber, which is valuable for mitigating the fiber nonlinearity effects and improves the technique adaptability for wavelength division multiplex (WDM) scenarios.

3. Experimental setup

The experimental setup for evaluating the converged fiber-wireless access network based on the free-running laser/envelope detection-enabled mmWave signal generation/detection is illustrated in Fig. 2.

An orthogonal frequency division multiplexing (OFDM) signal, which is digitally up-converted to a 2 GHz intermediate frequency (IF), is produced by an arbitrary waveform generator (AWG, Keysight M8195A) operating at 64 GS/s. The signal's spectrum is measured by an electrical spectrum analyzer (ESA, Rohde & Schwarz FSW43) and shown in inset (i) of Fig. 2. In generating the OFDM IF signal, a real-valued baseband OFDM signal containing 15 16-quadrature amplitude modulation (QAM)-encoded data-carrying subcarriers is first generated using a 32-point inverse fast Fourier transform (IFFT) operation based on the Hermitian symmetry. The OFDM cyclic prefix is 12.5%. The generated baseband OFDM signal is then oversampled by a factor of 64 to adjust the OFDM signal bandwidth to 0.5 GHz. Finally, the produced baseband OFDM signal is digitally up-converted to the desired IF region, followed by a digital signal clipping operation by a clipping ratio of 14 dB. The produced electrical OFDM signal has a bit rate of 1.67 Gbit/s, a bandwidth of 1 GHz at 2 GHz IF, and an amplitude of 500 mV_{pp}.

At the central office-BBU (CO-BBU), an optical intensity transmitter (Thorlabs MX35D) containing a 10 kHz linewidth external cavity laser (ECL)-based free-running tunable laser (TL-1), a RF electrical amplifier (EA), and a 35 GHz Mach-Zehnder modulator (MZM), is

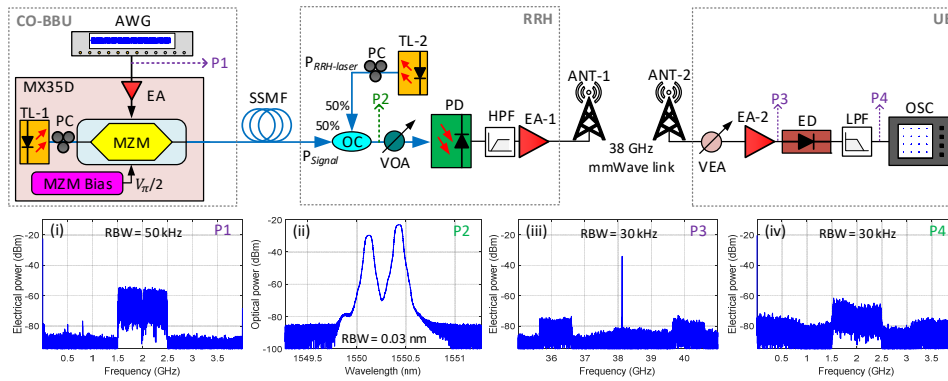


Fig. 2. Experimental setup for the proposed converged fiber-wireless access network. Insets show optical and electrical spectra at different points depicted in the experimental setup: (i) at P1, (ii) at P2, (iii) at P3, and (iv) at P4. ANT: antenna, TL: tunable laser, MZM: Mach-Zehnder modulator, AWG: arbitrary waveform generator, EDFA: erbium-doped fiber amplifier, OBPF: optical band-pass filter, SSMF: standard single-mode fiber, OC: optical coupler, VOA: variable optical attenuator, EA: electrical amplifier, VEA: variable electrical attenuator, HPF: high-pass filter, LPF: low-pass filter, ED: envelope detector, OSC: oscilloscope, PC: polarization controller, UE: user equipment, RBW: resolution bandwidth.

employed for electrical-optical (E-O) conversion. TL-1 generates a 13.5 dBm optical carrier at 1550.116 nm which is modulated by the MZM biased at the quadrature point by a voltage of $-1.549 V_{DC}$. The electrical OFDM signal is boosted by a 21 dB gain by the MX35D-embedded RF EA before driving the MZM. The optical signal launched into the fiber (P_{BBU}) has a power of 4 dBm. No optical amplifier is used at the CO-BBU.

After 25 km SSMF transmission, at the RRH, the received optical signal power is -1.5 dBm. A standalone ECL-based free-running TL-2 (Thorlabs TLX1) with a 10 kHz linewidth, is employed to generate a 1550.420 nm optical carrier with an optical power of 0 dBm ($P_{RRH-laser}$). This RRH locally-generated optical carrier has a frequency gap of 38 GHz relative to TL-1 (the BBU-laser). The RRH-received optical signal is passively combined with the TL-2 optical signal, and the resulting optical signal spectrum at point P2, measured by an optical spectrum analyzer (OSA, Anritsu MS9740B), is shown in inset (ii) of Fig. 2. A variable optical attenuator (VOA, Thorlabs EVOA1550A) is then employed to adjust the received total optical power (RoP) of the combined signals launched into the 40 GHz PD with a 0.7 A/W responsivity (Thorlabs RXM40AF). The optical beating in the PD results in the generation of a 38 GHz mmWave signal, which contains two OFDM sidebands at 36 GHz and 40 GHz conveying the same data. Afterward, the generated electrical mmWave signal passes through a 26–50 GHz electrical high-pass filter (HPF, Marki Microwave FH2600) to reduce the noise and remove the first three low-frequency signal terms in Eq. (4). The resultant signal is then amplified by a 0.01–47 GHz EA-1 (AT Microwave AT-BB-0047-2720C) with a 27 dB gain before wireless transmission over a distance of 5 m. The wireless link employs two antennas (ANT-1 and ANT-2, Mi-Wave 261A-25/599) with a 25 dBi gain, operating within a radio frequency range of 26.5–40 GHz.

After wireless transmission, at the UE, the received mmWave signal power is dynamically adjusted by a variable electrical attenuator (VEA) followed by a 20–44 GHz EA-2 (Evarant SBL-2034433040-2F2F-S1) with a 30 dB gain. The VEA introduces a 5 dB power attenuation and a ~ 5.6 dB insertion loss. The resulting signal spectrum is displayed in inset (iii) of Fig. 2. Slight frequency response distortions are observed in the upper OFDM sideband, which are mainly due to the 40 GHz PD bandwidth limitation. The mmWave signal is then directly down-converted using a 33–50 GHz ED (Spacek Labs DQ-2P) and then filtered by a 4 GHz

low-pass filter (LPF, Mini-Circuits ZLSS-4G-S+). The resulting signal spectrum is illustrated in inset (iv) of Fig. 2. Finally, the electrical signal is digitized by an oscilloscope (OSC, Keysight UXR0592A) operating at 8 GS/s, and finally processed offline for signal demodulation using conventional OFDM demodulation procedures, after the digital-domain IF-down-conversion operation, without estimating and compensating the carrier/subcarrier phase noise and frequency drifting effects.

To evaluate the transmission performances, here three cases are considered: Case-1 considers an optical back-to-back (oB2B) link, where the fiber and wireless links are excluded (ANTs and EA-2 are replaced with a high bandwidth, low loss RF coaxial cable). In this link, after the optical beating, electrical filtering and amplification, the produced mmWave signal is directly launched into the ED for demodulation; Case-2 considers a 25 km SSMF link, whose experimental setup is similar to Case-1 except that the OFDM signal is transmitted over 25 km SSMF. Note that in this case the wireless link, ANTs and EA-2 are also excluded. Case-3 involves the transmission of the signal over both the 25 km SSMF and the 5 m mmWave wireless links.

4. Experimental results and discussion

4.1. Transmission performance

Utilizing the experimental setup explicitly detailed in Section 3, when considering a mmWave frequency of 38 GHz, the measured bit error ratio (BER) performances versus RoP are shown in Fig. 3, where the RoP is the total optical power launched into the PD for generating the mmWave signal at the RRH.

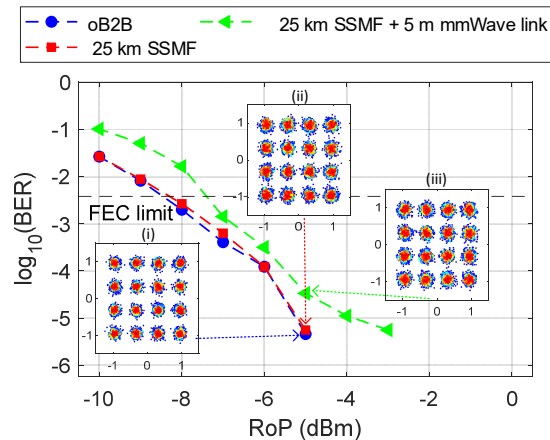


Fig. 3. BER performance versus RoP. Insets (i)–(iii) show the measured constellations at a fixed RoP of -5 dBm. The RoP contains RRH-received optical signal power and RRH-embedded free-running laser output power.

As seen in Fig. 3, Case-1 and Case-2 show similar BER performances, indicating that the fiber transmission-induced performance degradations are almost negligible. In comparison with Case-1 and Case-2, Case-3 exhibits a performance penalty of <1.15 dB at a BER of 3.8×10^{-3} which is the adopted 7% overhead hard-decision forward error correction (HD-FEC) limit [48]. Such a power penalty is mainly caused by the 5 m mmWave wireless link which requires electrical amplification to compensate for the free-space path loss. The impact of the mmWave wireless link transmission can also be observed by comparing the obtained results of Case-2 and Case-3. The insets in Fig. 3 show the constellations for each case at a fixed RoP of -5 dBm.

4.2. mmWave frequency tunability

Using the experimental setup Case-3 (25 km SSMF + 5 m mmWave wireless links), by simply adjusting the RRH-embedded TL-2 laser wavelength, different mmWave frequencies can be generated by the optical beating process, without reconfiguring any other electrical/optical devices. For different mmWave frequencies of 35 GHz, 38 GHz, and 41 GHz, Fig. 4(a) shows their BER performances after transmitting over 25 km SSMF + 5 m mmWave wireless links. The results demonstrate an achievable ± 3 GHz mmWave signal central frequency tuning range relative to 38 GHz, with transmission performance variations of < 1.2 dB at the FEC limit.

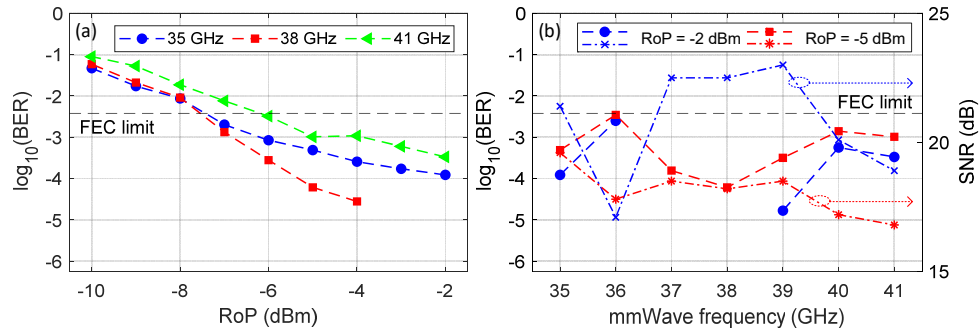


Fig. 4. (a) BER performance versus RoP at 35 GHz, 38 GHz, and 41 GHz mmWave frequencies, and (b) mmWave frequency tunability (dashed line – BER, left y-axis; dash-dotted line – SNR, right y-axis).

To further evaluate the mmWave frequency tunability, Fig. 4(b) shows the achievable BER performances using mmWave frequencies from 35 GHz to 41 GHz with fixed RoPs of -2 dBm and -5 dBm. Additionally, the observed signal-to-noise ratios (SNRs) are also plotted on the right y-axis of Fig. 4(b). As expected, the measured BER performances across the considered mmWave frequency range remain below the FEC limit. However, a slight BER performance degradation is observed at 36 GHz, attributed to the relatively low SNR of the received OFDM signal at 36 GHz. The SNR reduction is mainly due to the overall frequency response of the ED, HPF and the pre-/post-EAs. Additionally, the employed PD with a 3-dB bandwidth of 40 GHz causes noticeable BER/SNR degradations for mmWave frequencies of ≥ 40 GHz. Adopting advanced optical/electrical devices with flat frequency responses and wider bandwidths could enable a wider mmWave frequency tuning range.

4.3. Dynamic RRH-laser output power adjustment impact

From the theoretical analysis in Section 2, it is concluded that the power of the recovered signal after the ED is determined by both the optical data signal power received at the RRH and the output power of the RRH-laser. This implies the possibility of dynamically and flexibly controlling the RRH-laser output power to adaptively change the produced mmWave signal powers for achieving improved transmission performances and flexible mmWave coverages.

To confirm the above statement, using the experimental setup Case-3 (25 km SSMF + 5 m mmWave wireless links), the impact of dynamic variations in the output power of the RRH-laser ($P_{\text{RRH-laser}}$), TL-2, on the BER performance is investigated and illustrated in Fig. 5(a). The measured RoPs are also displayed on the right y-axis of Fig. 5(a). Additionally, the corresponding SNRs of the received OFDM signal after envelope detection are plotted in Fig. 5(b). In obtaining these results, the adopted mmWave frequency is 38 GHz, and the RRH-received optical signal power (P_{signal}) is controlled by adjusting the output power of the CO-BBU-laser.

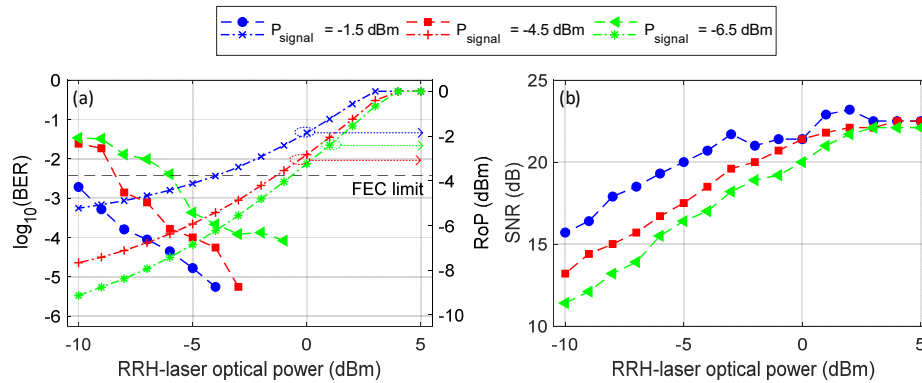


Fig. 5. (a) Impact of RRH-laser output power on BER performance for different RRH-received optical signal powers (dashed line – BER, dash-dotted line – RoP), and (b) the corresponding SNR of the received signal after ED.

Fig. 5(a) indicates that increasing RRH-laser powers can effectively improve the transmission performance for any considered RRH-received optical signal powers. Similarly, increasing the power of the RRH-received optical signal can enhance the transmission performance for any considered RRH-laser powers. The results agree with the theoretical analysis in Section 2, this suggests that increasing either the RRH-received optical signal power or the RRH-laser output power can enhance the resulting mmWave signal power, thus further improving the SNR of the UE-received OFDM signal, as confirmed in Fig. 5(b). Therefore, the results verify that dynamic RRH-laser output power adjustments are beneficial for improving the transmission performance and increasing the SNR. This potentially enables the BBU to launch low-power optical signals to fibers for reducing the associated fiber nonlinearity effects. Additionally, this also relaxes the need for additional post-detection EAs, thereby further potentially increasing signal SNRs.

4.4. Wireless network coverage

To identify the potential maximum achievable network coverage and further evaluate the dynamic RRH-laser output power adjustment-induced wireless network coverage flexibility, the experimental setup Case-3 (25 km SSMF + 5 m mmWave wireless links) is used to explore the transmission performances of the considered OFDM signal for different RRH-laser output powers and different mmWave wireless link distances. The adopted mmWave frequency is 38 GHz, and the fiber transmission distance is 25 km. For mmWave wireless distances of ≤ 10 m, a physical mmWave link is used. For each considered physical mmWave link length, VEA is adaptively adjusted to achieve optimum BER performances in the UE. Whereas, for distances of > 10 m, due to the indoor laboratory space limitation, a 10 m physical mmWave link is employed with an additional attenuation (introduced by the VEA) to offer an extra mmWave wireless link power loss based on the equivalent free-space path loss estimation [49]. Three RRH-laser output powers ($P_{\text{RRH-laser}}$) are considered: -3 dBm, 0 dBm, and 3 dBm, resulting in total RoPs at the PD of -3.4 dBm, -2 dBm, and 0 dBm, respectively.

The obtained results depicted in Fig. 6 demonstrate that increasing the RRH-laser output power effectively extends the maximum achievable mmWave signal transmission distance. For instance, with a low RRH-laser output power of -3 dBm (RoP = -3.4 dBm), the maximum achievable mmWave wireless link coverage, at the adopted FEC limit, is 21.2 m, while increasing the RRH-laser output power to 3 dBm (RoP = 0 dBm) would extend the maximum mmWave wireless link coverage of up to 45 m. Thus, a 6 dB increase in the RRH-laser output power (or a 3.4 dB increase in the RoP) results in an extended wireless coverage range of 23.8 meters. It is also

worth pointing out that the results in Fig. 6 are obtained by only adjusting the RRH-laser output power without reconfiguring any other optical/electrical components.

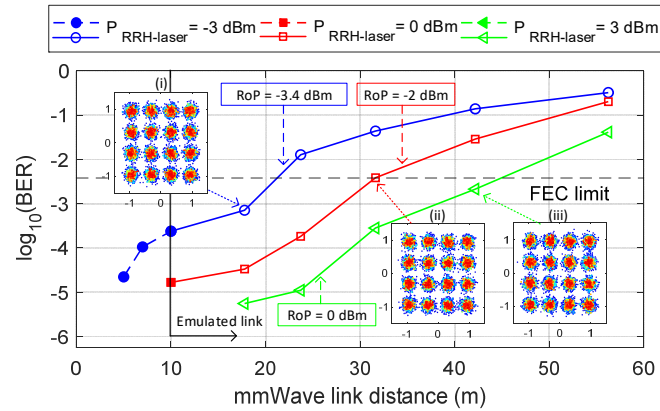


Fig. 6. The BER performance versus mmWave link distance for different RRH-laser optical powers. Insets show the measured constellations at the maximum achievable wireless transmission distance for each RRH-laser output power.

The above results indicate that the system may be suitable for 5G networks including femtocells for outdoor/indoor coverage. In addition, the results presented in this section and in Section 4.2 also imply that dynamic RRH-laser output power and wavelength adjustment offers a simple and effective way of flexibly and adaptively changing the wireless network coverage and mmWave frequency, this can be advantageous for inter-cell interference coordination (ICIC) to reduce its inter-cell interference.

4.5. System performance robustness and stability

In Section 2, the theoretical analysis shows that envelope detection offers mmWave carrier frequency drifting- and phase noise-insensitive mmWave down-conversion. This feature considerably relaxes the stringent requirement of deploying narrow linewidth lasers at the RRHs. To confirm the above statement, the BER performances using two RRH lasers with different linewidths are evaluated in Fig. 7, which shows the BER performances, for the three considered cases, using an RRH-laser with either a 10 kHz linewidth ECL (Thorlabs TLX1) or a 2 MHz linewidth distributed-feedback (DFB) laser (LD-PD PL-DFB-1550-C-1-PA-14BF) with the same wavelength and output power. The mmWave carrier frequency is ~ 38 GHz. In the figure, similar BER results obtained using the two different lasers with different linewidths are observed, thus confirming the validity of the statement.

Furthermore, in addition to the impact of the laser linewidth, the use of two independent free-running lasers respectively at the BBU and RRH also results in unwanted time-dependent carrier frequency drifting of the produced mmWave signals. Using the two different RRH-lasers mentioned above in the 25 km SSMF + 5 m mmWave wireless links, Fig. 8 shows the resultant mmWave carrier frequency drifting of the produced mmWave carrier over a 15-minute duration. The measurements are obtained by repeatedly and continuously measuring the carrier frequency locations and the maximum amplitudes of the mmWave carrier signal received at the UE before envelope detection. The resulting mmWave carrier frequency drifting, when the ECL laser (Fig. 8(a)) is utilized, is approximately 47 MHz, while the use of the DFB laser (Fig. 8(b)) exhibits a higher mmWave carrier frequency drifting of 155 MHz. The results indicate that, compared to the ECL lasers, the use of the DFB lasers not only introduces relatively large phase noise but also leads to a large mmWave carrier frequency drifting.

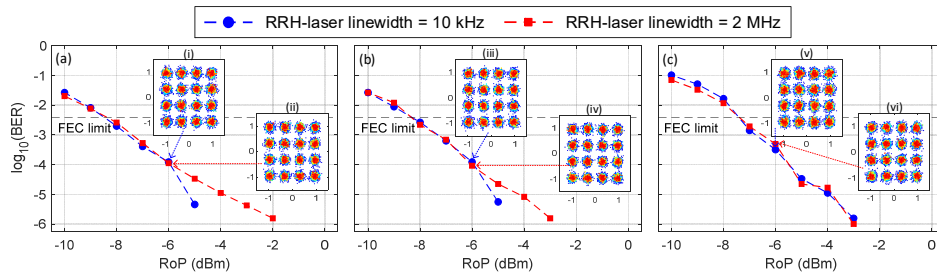


Fig. 7. BER versus RoP performance for using different RRH-laser linewidths for (a) oB2B, (b) 25 km SSMF, and (c) 25 km SSMF + 5 m mmWave wireless links. Insets show the measured constellations at a fixed RoP of -6 dBm: (i), (iii) and (v) are for RRH-laser with 10 kHz linewidth, and (ii), (iv) and (vi) are for RRH-laser with 2 MHz linewidth, respectively.

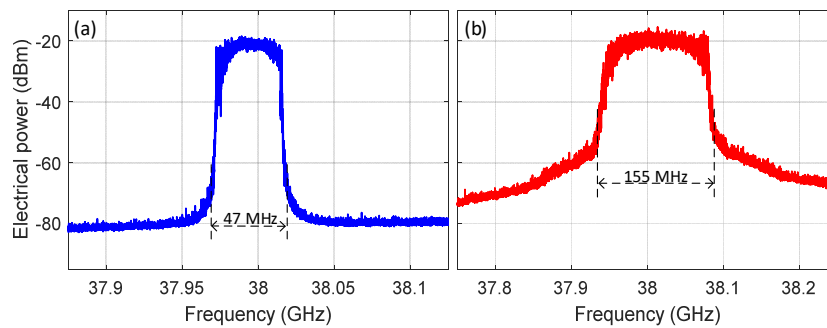


Fig. 8. Frequency drifting of produced mmWave carrier for RRH employing (a) 10 kHz linewidth ECL laser and (b) 2 MHz linewidth DFB laser.

However, despite the frequency drifting and linewidth differences, both types of lasers exhibit similar BER performances, as shown in Fig. 9. In obtaining these measurements, the RoP is fixed at -5 dBm, the mmWave frequency is set at 38 GHz, and the BER performances of the considered OFDM signal after transmission over the 25 km SSMF + 5 m mmWave wireless links are observed over a time duration of 20-minutes. The results suggest that this converged fiber-wireless access network possesses excellent performance stability and allows RRHs to use low-cost MHz-linewidth-level free-running lasers to reduce the overall network capital expenditure.

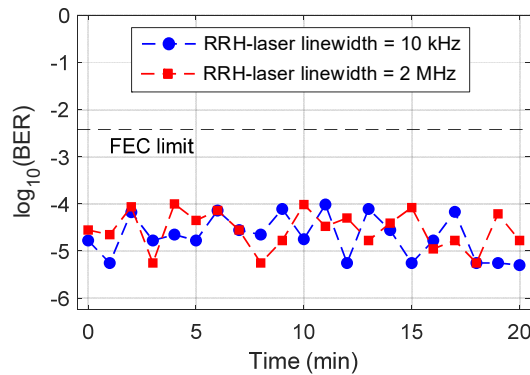


Fig. 9. Performance stability observed over 20 minutes.

5. Conclusions

This paper has experimentally investigated the performances of the cost-effective seamlessly converged fiber-wireless access network, which employs a free-running laser at each RRH for generating mmWave signals via optical beating between the RRH-laser and the BBU transmitted optical signal, and uses an electrical passive envelope detector at the UE for realizing a cost-effective LO-free mmWave signal detection. In the considered 1.67 Gbit/s @38 GHz converged fiber-wireless access network with a 25 km SSMF transmission and 5 m mmWave wireless links, the obtained experimental results show that dynamic adjustments of the RRH-laser output wavelength and power not only improve the transmission performance but also offer excellent mmWave carrier frequency tunability within a wide frequency range, and also provide adaptive wireless coverage. For the experimental demonstrations, the maximum achievable wireless network coverage could potentially be extended from 21.2 m to >45 m by increasing the RRH-laser output power by ~6 dB. Additionally, the results also confirm that the considered seamlessly converged fiber-wireless access network possesses excellent performance stability and allows RRHs to adopt low-cost MHz-level-linewidth free-running lasers without implementing extra techniques in the UE receivers to mitigate the phase noise and frequency drifting effects.

Funding. UK Research and Innovation, Engineering and Physical Sciences Research Council (Project TITAN, [EP/Y037243/1]); Department for Science, Innovation and Technology, Future Open Networks Research Challenge (Project REASON); Welsh Government and the UK Government (North Wales Growth Deal through Ambition North Wales); Sichuan Province Science and Technology Support Program (2023YFH0067).

Disclosures. The authors declare no conflicts of interest.

Data availability. Data underlying the results presented in this paper are not publicly available at this time but may be obtained from the authors upon reasonable request.

References

1. GSMA, "The Mobile Economy 2024," 2024.
2. Z. Zhang, Y. Xiao, Z. Ma, *et al.*, "6 G Wireless Networks: Vision, Requirements, Architecture, and Key Technologies," *IEEE Veh. Technol. Mag.* **14**(3), 28–41 (2019).
3. W. Jiang, B. Han, M. A. Habibi, *et al.*, "The Road Towards 6G: A Comprehensive Survey," *IEEE Open J. Commun. Soc.* **2**, 334–366 (2021).
4. H. Rodrigues Dias Filgueiras, E. Saia Lima, M. Seda Borsato, *et al.*, "Wireless and Optical Convergent Access Technologies Toward 6G," *IEEE Access* **11**, 9232–9259 (2023).
5. M. Sung, S. Kim, E.-S. Kim, *et al.*, "Photonic THz Communications Based on Radio-Over-Fiber Technology for 6 G Mobile Network: Design and Opportunity," *IEEE J. Sel. Top. Quantum Electron.* **29**(5: Terahertz Photonics), 1–11 (2023).
6. ETSI, "TS 138 101-1 - V17.12.0 - 5 G; NR; User Equipment (UE) radio transmission and reception; Part 1: Range 1 Standalone," 2024.
7. X. Wang, L. Kong, F. Kong, *et al.*, "Millimeter Wave Communication: A Comprehensive Survey," *IEEE Commun. Surv. Tut.* **20**(3), 1616–1653 (2018).
8. X. Li, J. Yu, and G.-K. Chang, "Photonics-Aided Millimeter-Wave Technologies for Extreme Mobile Broadband Communications in 5 G," *J. Lightwave Technol.* **38**(2), 366–378 (2020).
9. W. Hong, Z. H. Jiang, C. Yu, *et al.*, "The Role of Millimeter-Wave Technologies in 5 G/6 G Wireless Communications," *IEEE J. Microw.* **1**(1), 101–122 (2021).
10. P. Li, L. Zhu, H. Wang, *et al.*, "One-Shot Blind Frequency-Domain Nonlinear Equalization for Millimeter-Wave Fiber-Wireless IFoF Mobile Fronthaul System," *J. Lightwave Technol.* **41**(14), 4624–4634 (2023).
11. J. Yao, "Microwave Photonics," *J. Lightwave Technol.* **27**(3), 314–335 (2009).
12. A. B. Dar and F. Ahmad, "Optical millimeter-wave generation techniques: An overview," *Optik* **258**, 168858 (2022).
13. H.-J. Song and N. Lee, "Terahertz Communications: Challenges in the Next Decade," *IEEE Trans. Terahertz Sci. Technol.* **12**(2), 105–117 (2022).
14. H.-Y. Wang, C.-H. Cheng, B. Su, *et al.*, "Ultrahigh Capacity MMWoF Link Using 2- λ VCSEL Front-Haul Transmitter Encoded With Broadband Generalized FDM Data Stream," *J. Lightwave Technol.* **41**(10), 3007–3016 (2023).
15. Z. Liu and R. Slavik, "Optical Injection Locking: From Principle to Applications," *J. Lightwave Technol.* **38**(1), 43–59 (2020).
16. K. Balakier, H. Shams, M. J. Fice, *et al.*, "Optical Phase Lock Loop as High-Quality Tuneable Filter for Optical Frequency Comb Line Selection," *J. Lightwave Technol.* **36**(19), 4646–4654 (2018).
17. L. Zhang, X. Xin, B. Liu, *et al.*, "OFDM Modulated WDM-ROF System based on PCF-Supercontinuum," *Opt. Express* **18**(14), 15003–15008 (2010).

18. D. Dass, A. Delmade, L. Barry, *et al.*, "Wavelength & mm-Wave Flexible Converged Optical Fronthaul With a Low Noise Si-Based Integrated Dual Laser Source," *J. Lightwave Technol.* **40**(10), 3307–3315 (2022).
19. M. Zhao, W. Zhou, L. Zhao, *et al.*, "A New Scheme to Generate Multi-Frequency Mm-Wave Signals Based on Cascaded Phase Modulator and I/Q Modulator," *IEEE Photonics J.* **11**(5), 1–8 (2019).
20. H. Zhang, L. Cai, S. Xie, *et al.*, "A Novel Radio-Over-Fiber System Based on Carrier Suppressed Frequency Eightfold Millimeter Wave Generation," *IEEE Photonics J.* **9**(5), 1–6 (2017).
21. P.-T. Shih, J. J. Chen, C.-T. Lin, *et al.*, "Optical millimeter-wave signal generation via frequency 12-tupling," *J. Lightwave Technol.* **28**(1), 71–78 (2010).
22. T. Schneider, D. Hannover, and M. Junker, "Investigation of Brillouin scattering in optical fibers for the generation of Millimeter waves," *J. Lightwave Technol.* **24**(1), 295–304 (2006).
23. J. Shi, Y. Wang, J. Zhang, *et al.*, "Beyond 500 GHz THz Wireless Links Based on Heterodyne Photo-mixing and Absolute Operation Pruned Two-Stage MIMO Volterra," *IEEE Trans. Terahertz Sci. Technol.* **14**(3), 364–376 (2024).
24. L. Gonzalez-Guerrero, M. Ali, R. Guzman, *et al.*, "Photonic Sub-Terahertz IM Links: Comparison Between Double and Single Carrier Modulation," *J. Lightwave Technol.* **40**(18), 6064–6070 (2022).
25. I. Gonzalez Insua, D. Plettemeier, and C. G. Schaffer, "Simple Remote Heterodyne Radio-Over-Fiber System for Gigabit Per Second Wireless Access," *J. Lightwave Technol.* **28**(16), 2289–2295 (2010).
26. M. Zhu, L. Zhang, J. Wang, *et al.*, "Radio-Over-Fiber Access Architecture for Integrated Broadband Wireless Services," *J. Lightwave Technol.* **31**(23), 3614–3620 (2013).
27. H.-H. Lu, C.-Y. Li, W.-S. Tsai, *et al.*, "Two-Way 5 G NR Fiber-Wireless Systems Using Single-Carrier Optical Modulation for Downstream and Phase Modulation Scheme for Upstream," *J. Lightwave Technol.* **41**(6), 1749–1758 (2023).
28. L. Gonzalez-Guerrero, H. Shams, I. Fatadin, *et al.*, "Single Sideband Signals for Phase Noise Mitigation in Wireless THz-Over-Fiber Systems," *J. Lightwave Technol.* **36**(19), 4527–4534 (2018).
29. L. Gonzalez-Guerrero and G. Carpintero, "Coherent photonic Terahertz transmitters compatible with direct comb modulation," *Sci. Rep.* **12**(1), 1–10 (2022).
30. A. H. M. Razibul Islam, M. Bakaul, A. Nirmalathas, *et al.*, "Millimeter-Wave Radio-Over-Fiber System Based on Heterodyned Unlocked Light Sources and Self-Homodyned RF Receiver," *IEEE Photonics Technol. Lett.* **23**(8), 459–461 (2011).
31. R. Sambaraju, D. Zibar, A. Caballero, *et al.*, "100-GHz Wireless-Over-Fiber Links With Up to 16-Gb/s QPSK Modulation Using Optical Heterodyne Generation and Digital Coherent Detection," *IEEE Photonics Technol. Lett.* **22**(22), 1650–1652 (2010).
32. C.-T. Tsai, C.-C. Li, C.-H. Lin, *et al.*, "Long-reach 60-GHz MMWoF link with free-running laser diodes beating," *Sci. Rep.* **8**(1), 13711 (2018).
33. J. Shi, Z. Li, J. Jia, *et al.*, "Waveform-to-Waveform End-to-End Learning Framework in a Seamless Fiber-Terahertz Integrated Communication System," *J. Lightwave Technol.* **41**(8), 2381–2392 (2023).
34. L. Gonzalez-Guerrero, R. Guzman, M. Ali, *et al.*, "Injection Locking Properties of an Dual Laser Source for mm-Wave Communications," *J. Lightwave Technol.* **40**(20), 6685–6692 (2022).
35. S. E. Alavi, M. R. K. Soltanian, I. S. Amiri, *et al.*, "Towards 5G: a photonic base millimeter wave signal generation for applying in 5 G access fronthaul," *Sci. Rep.* **6**(1), 19891 (2016).
36. K. Zeb, Z. Lu, J. Liu, *et al.*, "Broadband Optical Heterodyne Millimeter-Wave-over-Fiber Wireless Links Based on a Quantum Dash Dual-Wavelength DFB Laser," *J. Lightwave Technol.* **40**(12), 3698–3708 (2022).
37. R. Guzman, L. Gonzalez, A. Zarzuelo, *et al.*, "Widely Tunable RF Signal Generation Using an InP/Si3N4 Hybrid Integrated Dual-Wavelength Optical Heterodyne Source," *J. Lightwave Technol.* **39**(24), 7664–7671 (2021).
38. F. Zhao, J. L. Li, K. M. Gong, *et al.*, "80-GHz RoF Based on Push-Pull Modulator," *IEEE Photonics J.* **11**(5), 1–6 (2019).
39. J. L. Li, F. Zhao, and J. Yu, "D-band Millimeter Wave Generation and Transmission Through Radio-Over-Fiber System," *IEEE Photonics J.* **12**(6), 1–8 (2020).
40. M. Morant, L. Gonzalez-Guerrero, C. C. Renaud, *et al.*, "Remote Photonic THz Generation Using an Optical Frequency Comb and Multicore Fiber," *J. Lightwave Technol.* **39**(24), 7621–7627 (2021).
41. M. Botella-Campos, J. Mora, and B. Ortega, "On the Use of a Directly Modulated Laser in a Phase Modulated-Assisted mmW Signal Generation and Transmission Link," *J. Lightwave Technol.* **41**(24), 7390–7398 (2023).
42. A. Sun, Z. Li, B. Dong, *et al.*, "End-to-End Deep-Learning-Based Photonic-Assisted Multi-User Fiber-mmWave Integrated Communication System," *J. Lightwave Technol.* **42**(1), 80–94 (2024).
43. X. Li, Y. Xu, and J. Yu, "Over 100-Gb/s V-Band Single-Carrier PDM-64QAM Fiber-Wireless-Integration System," *IEEE Photonics J.* **8**(5), 1–7 (2016).
44. X. Li, J. Yu, L. Zhao, *et al.*, "1-Tb/s Photonics-aided Vector Millimeter-Wave Signal Wireless Delivery at D-Band," *Optical Fiber Communications Conference and Exhibition (OFC)*, 2018.
45. W. Tong, J. Zhang, M. Zhu, *et al.*, "Experimental Comparison of Single-Carrier and Digital Subcarrier Multiplexing Transmissions in a W-Band 200 Gb/s Fiber-Wireless System Considering Transmitter IQ Imbalance and Skew Mitigation," *IEEE Photonics J.* **15**(4), 1–8 (2023).
46. B. Dong, J. Jia, L. Tao, *et al.*, "Photonic-Based W-Band Integrated Sensing and Communication System With Flexible Time-Frequency Division Multiplexed Waveforms for Fiber-Wireless Network," *J. Lightwave Technol.* **42**(4), 1281–1295 (2024).

47. J. Li, Y. Cai, S. Xiang, *et al.*, “Laser Phase Noise Tolerant and Power-Fading-Free Hybrid Fiber-Wireless Double-Sideband Transmission With Spectral Efficiency Enhancement,” *IEEE Photonics J.* **16**(6), 1–6 (2024).
48. H. Xin, K. Zhang, L. Li, *et al.*, “50 Gbps PAM-4 Over Up to 80-km Transmission With C-Band DML Enabled by Post-Equalizer,” *IEEE Photonics Technol. Lett.* **32**(11), 643–646 (2020).
49. J. G. Proakis and M. Salehi, *Digital Communications*, 5th ed. (McGraw-Hill, 2008).